Radboud Repository

Radboud University Nijmegen

PDF hosted at the Radboud Repository of the Radboud University Nijmegen

The following full text is a publisher's version.

For additional information about this publication click this link.
http://hdl.handle.net/2066/70933

Cellular/Molecular

NaV1.7 Gain-of-Function Mutations as a Continuum: A1632E Displays Physiological Changes Associated with Erythromelalgia and Paroxysmal Extreme Pain Disorder Mutations and Produces Symptoms of Both Disorders

M. Estacion,[1,2,3] **S. D. Dib-Hajj,**[1,2,3] **P. J. Benke,**[4] **Rene H. M. te Morsche,**[5] **E. M. Eastman,**[1,2,3] **L. J. Macala,**[1,2,3] **J. P. H. Drenth,**[5] **and S. G. Waxman**[1,2,3]

[1]Department of Neurology and [2]Center for Neuroscience and Regeneration Research, Yale University School of Medicine, New Haven, Connecticut 06510, [3]Rehabilitation Research Center, Veterans Affairs Connecticut Healthcare System, West Haven, Connecticut 06516, [4]Department of Genetics, Joe DiMaggio Children's Hospital, Hollywood, Florida 33021, and [5]Department of Gastroenterology and Hepatology, Radboud University Nijmegen Medical Center, 6500 HB Nijmegen, The Netherlands

Gain-of-function mutations of NaV1.7 have been shown to produce two distinct disorders: NaV1.7 mutations that enhance activation produce inherited erythromelalgia (IEM), characterized by burning pain in the extremities; NaV1.7 mutations that impair inactivation produce a different, nonoverlapping syndrome, paroxysmal extreme pain disorder (PEPD), characterized by rectal, periocular, and perimandibular pain. Here we report a novel NaV1.7 mutation associated with a mixed clinical phenotype with characteristics of IEM and PEPD, with an alanine 1632 substitution by glutamate (A1632E) in domain IV S4–S5 linker. Patch-clamp analysis shows that A1632E produces changes in channel function seen in both IEM and PEPD mutations: A1632E hyperpolarizes (-7 mV) the voltage dependence of activation, slows deactivation, and enhances ramp responses, as observed in NaV1.7 mutations that produce IEM. A1632E depolarizes ($+17$mV) the voltage dependence of fast inactivation, slows fast inactivation, and prevents full inactivation, resulting in persistent inward currents similar to PEPD mutations. Using current clamp, we show that A1632E renders dorsal root ganglion (DRG) and trigeminal ganglion neurons hyperexcitable. These results demonstrate a NaV1.7 mutant with biophysical characteristics common to PEPD (impaired fast inactivation) and IEM (hyperpolarized activation, slow deactivation, and enhanced ramp currents) associated with a clinical phenotype with characteristics of both IEM and PEPD and show that this mutation renders DRG and trigeminal ganglion neurons hyperexcitable. These observations indicate that IEM and PEPD mutants are part of a physiological continuum that can produce a continuum of clinical phenotypes.

Key words: sodium channel; neuropathic pain; sensory neuron; voltage-clamp; current-clamp; dorsal root ganglion

Introduction

It is now clear that there are nine different isoforms of voltage-gated sodium channels, all sharing a common overall motif but with distinct amino acid sequences and different physiological and pharmacological properties (Catterall et al., 2005). NaV1.7 sodium channels are unique in that they are preferentially expressed within primary sensory neurons of dorsal root (DRG) and trigeminal ganglion and sympathetic ganglion neurons (Felts et al., 1997; Sangameswaran et al., 1997; Toledo-Aral et al., 1997),

especially within nociceptors (Djouhri et al., 2003), and display slow closed-state inactivation, a property that enables these channels to produce a depolarizing response to small slow depolarizations that are subthreshold with respect to the action potential (Cummins et al., 1998). The biophysical properties and subcellular distribution of NaV1.7 suggest that it functions to boost subthreshold stimuli, thereby setting the gain on nociceptors (Waxman, 2006; Rush et al., 2007).

Over the past few years, NaV1.7 has assumed a prominent role in pain research because mutations in this channel have been linked to inherited human pain syndromes (Dib-Hajj et al., 2007; Drenth and Waxman, 2007). Gain-of-function mutations (Yang et al., 2004; Dib-Hajj et al., 2005; Drenth et al., 2005; Michiels et al., 2005; Han et al., 2006; Lee et al., 2007) that shift activation of NaV1.7 in a hyperpolarizing direction, slow deactivation, and enhance ramp currents cause inherited erythromelalgia (IEM) (Cummins et al., 2004; Dib-Hajj et al., 2005; Choi et al., 2006; Han et al., 2006; Harty et al., 2006; Lampert et al., 2006; Sheets et

al., 2007; Cheng et al., 2008), a disorder in which patients experience severe burning pain in the feet and, in most cases, in the hands, in response to mild warmth and exercise. A different set of gain-of-function mutations that impair inactivation of Na$_V$1.7 and in some cases produce a persistent current (Fertleman et al., 2006; Dib-Hajj et al., 2008; Jarecki et al., 2008) has been linked to a different, nonoverlapping syndrome, paroxysmal extreme pain disorder (PEPD), characterized by paroxysmal episodes of burning pain in the rectal, ocular, and mandibular areas accompanied by autonomic manifestations such as skin flushing (Fertleman et al., 2006). In contrast, loss-of-function mutations of Na$_v$1.7 have been linked to congenital inability to experience pain (Cox et al., 2006; Ahmad et al., 2007; Goldberg et al., 2007).

In this paper, we describe and characterize a new mutation in Na$_V$1.7, A1632E, in a patient with a unique mixed clinical phenotype that includes characteristics of both IEM and PEPD. We show that this mutation produces changes in channel function that have been previously observed separately in both IEM and PEPD, shifting activation in a hyperpolarizing direction, slowing deactivation, and enhancing ramp currents as reported previously for IEM mutations and also impairing inactivation as previously reported for PEPD mutations. We also show that this mutation produces hyperexcitability within both DRG and trigeminal ganglion neurons.

Materials and Methods

Patient. The patient is a Caucasian 10-year-old female with a life-long pain syndrome with characteristics of both IEM and PEPD. The subject and parents gave written informed consent, and the study was approved by the Ethics Committee of the Hollywood Memorial Hospital (Hollywood, FL).

Exon screening. Genomic DNA was purified from venous blood. Genomic DNA from 92 Caucasian individuals was used as a normal population control. Coding exons and flanking intronic sequences, as well as exons encoding 5′ and 3′ untranslated sequences within the cDNA were amplified and sequenced as described previously (Drenth et al., 2005). Genomic sequences were compared with the reference Na$_v$1.7 cDNA (Klugbauer et al., 1995) to identify sequence variation.

Plasmid and stable cell line. The human Na$_V$1.7 insert was cloned into a mammalian expression vector (Klugbauer et al., 1995) and converted to become TTX-R (hNa$_V$1.7$_R$) by Y362S substitution (Herzog et al., 2003). The A1632E mutation was introduced into hNa$_V$1.7$_R$ using Quick-Change XL II site-directed mutagenesis (Stratagene). Transfected HEK 293 cells, grown under standard culture conditions (5% CO$_2$, 37°C) in DMEM supplemented with 10% fetal bovine serum, were treated with G418 for several weeks and stable cell lines that express the mutant channel were selected. Cells for voltage-clamp recordings were sparsely subplated onto 35 mm culture dishes.

Primary sensory neuron isolation and transfection. Dorsal root ganglia and trigeminal ganglia from Sprague Dawley rat pups (postnatal day 1–5) were isolated and then cultured using the same protocol. Dissected ganglia were placed in ice-cold oxygenated complete saline solution (CSS), which contained the following (in mM): 137 NaCl, 5.3 KCl, 1 MgCl$_2$, 25 sorbitol, 3 CaCl$_2$, and 10 HEPES, pH 7.2. They were then transferred to an oxygenated, 37°C CSS solution containing 1.5 mg/ml Collagenase A (Roche Applied Science) and 0.6 mM EDTA and incubated with gentle agitation at 37°C for 20 min. This solution was then exchanged with an oxygenated, 37°C CSS solution containing 1.5 mg/ml Collagenase D (Roche Applied Science), 0.6 mM EDTA, and 30 U/ml papain (Worthington Biochemicals) and was incubated with gentle agitation at 37°C for 20 min. The solution was then aspirated, and the ganglia were triturated in DRG media [DMEM/F-l2 (1:1) with 100 U/ml penicillin, 0.1 mg/ml streptomycin (Invitrogen), and 10% fetal calf serum (Hyclone), which contained 1.5 mg/ml bovine serum albumin (Sigma-Aldrich) and 1.5 mg/ml trypsin inhibitor (Roche Applied Science)].

Either wild-type hNa$_V$1.7$_R$ (WT) or hNa$_V$1.7$_R$–A1632E mutant channels were transiently transfected into the DRG or trigeminal ganglia neurons, along with enhanced green fluorescent protein (GFP), by electroporation with a Nucleofector II (Amaxa) using Rat Neuron Nucleofector Solution and program G-013. The ratio of sodium channel to GFP constructs was 5:1. The transfected neurons were allowed to recover for 5 min at 37°C in 0.5 ml of Ca^{2+}-free DMEM containing 10% fetal calf serum. The cell suspension was then diluted with DRG media containing 1.5 mg/ml bovine serum albumin and 1.5 mg/ml trypsin inhibitor, 80 μl was plated on 12 mm circular poly-D-lysine/laminin precoated coverslips (BD Biosciences), and the cells were incubated at 37°C in 5% CO$_2$ for 30 min. DRG media (1 ml/well), supplemented with 50 ng/ml each of mouse NGF (Alomone Labs) and glial cell line-derived neurotrophic factor (Peprotec), was then added, and the cells were maintained at 37°C in a 5% CO$_2$ incubator.

Electrophysiology. Whole-cell voltage-clamp recordings were performed using the following solutions. The extracellular solution contained the following (in mM): 140 NaCl, 3 KCl, 1 MgCl$_2$, 1 CaCl$_2$, and 10 HEPES, pH 7.3 with NaOH (adjusted to 320 mOsm with dextrose). The pipette solution contained the following (in mM): 135 Cs-aspartate, 10 NaCl, 2 MgCl$_2$, 0.1 CaCl$_2$, 1.1 EGTA, pCa 8, and 10 HEPES, pH 7.2 with CsOH (adjusted to 310 mOsm with dextrose). Patch pipettes had a resistance of 1–3 MΩ when filled with pipette solution. The junction potential of 16 mV (calculated by JPcalc included in pClamp software) was compensated by setting the holding potential during the seal test period to −16 mV. Once the seal had formed, these two solutions were no longer in contact and the applied potential was correct. After achieving the whole-cell recording configuration, the pipette and cell capacitance were manually minimized using the Axopatch 200B (Molecular Devices) compensation circuitry. To reduce voltage errors, 80–90% series resistance and prediction compensation was applied. Cells were excluded from analysis if the predicted voltage error exceeded 3 mV. The recorded currents were digitized using pClamp software (version 10) and a Digidata 1440A interface (Molecular Devices) at a rate of 50 kHz after passing through a low-pass Bessel filter setting of 10 kHz. Linear leak and residual capacitance artifacts were subtracted out using the P/N method provided by the Clampex software. The Na-current recordings were initiated after a 5 min equilibration period once whole-cell configuration was achieved.

Data analysis was performed using Clampfit (Molecular Devices) or Origin (Microcal Software). To generate activation curves, cells were held at −100 mV and stepped to potentials of −80 to +40 mV in 5 mV increments for 100 ms. Peak inward currents obtained from activation protocols were converted to conductance values using the equation, $G = I/(V_m - E_{Na})$, for which G is the conductance, I is the peak inward current, V_m is the membrane potential step used to elicit the response, and E_{Na} is the reversal potential for sodium (determined for each cell using the x-axis intercept of a linear fit of the peak inward current responses). Conductance data were normalized by the maximum conductance value and fit with a Boltzmann equation of the form $G = G_{min} + (G_{max} - G_{min})/(1 + \exp[(V_{1/2} - V_m)/k])$, where $V_{1/2}$ is the midpoint of activation, and k is a slope factor. To generate steady-state fast inactivation curves, cells were stepped to inactivating potentials of −170 to −30 mV for 500 ms followed by a 20 ms step to −20 mV. The protocol for slow inactivation consisted of a 30 s step to potentials varying from −120 to 10 mV, followed by a 100 ms step to −120 mV to remove fast inactivation and a 20 ms step to 0 mV to elicit a test response. Peak inward currents obtained from steady-state fast inactivation and slow inactivation protocols were normalized by the maximum current amplitude and fit with a Boltzmann equation of the form $I = I_{min} + (I_{max} - I_{min})/(1 + \exp[(V_m - V_{1/2})/k])$, where V_m represents the inactivating prepulse membrane potential, and $V_{1/2}$ represents the midpoint of inactivation. Decaying currents were fit with a single-exponential equation of the form $I = A * \exp(-t/\tau) + I_c$, where A is the amplitude of the fit, t is time, τ is the time constant of decay, and I_c is the asymptotic minimum to which the currents decay. Data are expressed as means ± SEM. Statistical significance was determined by Student's t test.

Whole-cell current-clamp recordings were performed using the Axopatch 200B amplifier, digitized using the Digidata 1440A interface, and controlled using pClamp software. The bath solution for current-clamp

recordings contained the following (in mM): 140 NaCl, 3 KCl, 1 MgCl$_2$, 1 CaCl$_2$, and 10 HEPES, pH 7.3 with NaOH (adjusted to 315 mOsm with dextrose). The pipette solution contained the following (in mM): 140 KCl, 0.5 EGTA, 5 HEPES, and 3 Mg-ATP, pH 7.3 with KOH (adjusted to 300 mOsm with dextrose). The junction potential between these two solutions given by JPcalc was 5 mV, but no correction was applied for current-clamp experiments. Recordings were performed on transfected presumptive nociceptive neurons based on the morphology of small-diameter (20–28 μm) round cell bodies that also exhibited GFP fluorescence. All recordings were performed between 20 and 30 h after transfection. Coverslips were transferred to a perfusable chamber (Warner Instruments) and all recordings were initiated within 1 h. Whole-cell configuration was obtained in voltage-clamp mode before proceeding to the current-clamp recording mode. Cells with stable (<10% variation) resting membrane potentials (RMPs) more negative than −35 mV and overshooting action potentials (>85 mV RMP to peak) were used for additional data collection. Input resistance was determined by the slope of a line fit to hyperpolarizing responses to current steps of 10–35 pA. Threshold was determined by the first action potential elicited by a series of depolarizing current injections that increased in 5 pA increments. Action potential frequency was determined by quantifying the number of action potentials elicited in response to depolarizing current injections of 1 s duration.

Results

Clinical phenotype and identification of the A1632E mutation

The patient presented with apnea, bradycardia, and poor feeding since birth. Severe reflux, projectile vomiting, and a hypersensitive gag reflex required a fundoplication and gastrostomy tube for management. Bradycardic episodes, in which the patient would turn blue and sometimes required cardiopulmonary resuscitation, were precipitated by touching or stimulation such as eating, voiding, or bowel movements, and required insertion of a pacemaker at 18 months of age. Rectal sensitivity continued and episodes of periodic pain and erythema developed as the patient grew older. After age 3, the patient developed almost daily attacks of (1) unilateral eye, jaw, or facial discomfort and redness, (2) episodes of harlequin (half-face) redness and facial pain, (3) stomach pain, vomiting, or breath-holding spells, and (4) transient episodes of pain described as "hot needles" and erythema in the feet, hands, and head, often precipitated by warmth or being touched, and attenuated by cooling. The parents and a half sibling are asymptomatic.

Amplification and direct sequencing of all exons of SCN9A identified a heterozygous 4895C > A mutation in exon 26 in the index patient, which predicts amino acid substitution A1632E in Na$_V$1.7. The mutation was not present in the unaffected father and mother, suggesting that this mutation appeared *de novo*. The 4895C > A mutation was absent in 92 unrelated healthy control subjects of the same ethnic origin. The A1632E mutation alters a highly conserved amino acid within the linker between transmembrane segments S4 and S5 of domain IV (Fig. 1). The amino acid sequence of this loop is highly conserved among all sodium channels except Na$_V$1.9, in which the residue corresponding to A1632 is replaced by a serine (Fig. 1). Na$_V$1.9 shows the most sequence variability compared with the other members of the sodium channel gene family (Dib-Hajj et al., 1998).

Voltage-clamp recordings from HEK 293 cells stably expressing WT or A1632E mutant hNa$_V$1.7$_R$ channels

Whole-cell voltage-clamp recordings were performed on clonal cell lines expressing either WT or A1632E channels. The activation properties of the currents expressed by these cells were tested by holding the cells at −100 mV and then applying 100 ms test pulses to potentials between −80 and +40 mV in 5 mV incre-
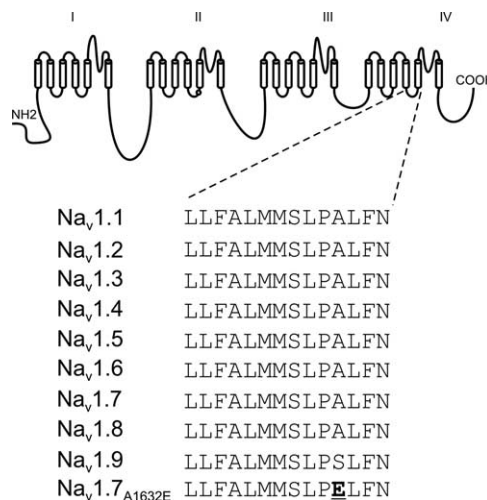
Figure 1. Sequence alignment of DIV/S4–S5 linker from human sodium channels. Schematic of the topology of the sodium channel polypeptide showing the location of the A1632E near the C-terminal end of the linker joining segments S4 and S5 in domain IV. The A1632E substitution is noted in the sequence from Na$_V$1.7. The equivalent residue is conserved in all sodium channels except for Na$_V$1.9, in which the analogous residue is a serine (S1496).

ments. Inward currents recorded by this protocol are shown for WT (Fig. 2A) and A1632E (Fig. 2B) channels. The average peak inward current was smaller for A1632E cells (0.95 ± 11 nA; n = 18) compared with WT cells (3.21 ± 0.41 nA; n = 9). This difference was maintained when normalized for capacitance to give a significant reduction in current density from the A1632E cells compared with WT cells (30.5 ± 3.8 pA/pF for A1632E; 152 ± 23 pA/pF for WT; p < 0.001). The amplitude of the current in HEK 293 cells transiently transfected with A1632E mutant channels was also smaller than that of HEK 293 cells transiently transfected with WT channels (data not shown), suggesting that the smaller current in the stable lines was not caused by the site of integration of the construct.

Time-to-peak and rate of deactivation

Examination of the mean time-to-peak (Fig. 2C) revealed a small increase in the time-to-peak for A1632E currents compared with WT currents, which was significant over the voltage range between −5 to +30 mV. An additional test for altered activation properties is to examine the deactivation kinetics as open channels transition back to the closed state. Single-exponential fits of the current decay (to measure time constant) showed that the A1632E channels close significantly more slowly over the entire voltage range from −100 to −40 mV (Fig. 2D)

Voltage dependence of activation and fast inactivation

The voltage dependence of activation and fast inactivation was examined by transforming the peak current versus voltage (*I–V*) curves into conductance versus voltage (*G–V*) curves as described in Materials and Methods. The *G–V* curve was fit to a Boltzmann function that directly gives the voltage midpoint ($V_{1/2}$) as well as the slope factor (k) of the voltage-dependent response. The Boltzmann fits for both activation and fast inactivation were derived for each cell individually. The averages of the normalized *G–V* curves for activation and fast inactivation for both A1632E and WT channels are illustrated in Figure 2E. The average of the fits for fast inactivation revealed that, like other PEPD mutant Na channels, the $V_{1/2}$ for A1632E channels was significantly shifted in the depolarizing direction compared with

WT (-63.9 ± 0.9 mV for A1632E, $n = 18$; -80.9 ± 1.4 mV for WT, $n = 9$; $p < 0.001$). In addition to this 17 mV shift in the depolarizing direction, the slope factor for A1632E fast inactivation became significantly steeper (5.61 ± 0.31 for A1632E; 8.13 ± 0.36 for WT; $p < 0.001$).

Comparing the average of the fits for the voltage dependence of activation revealed a shift, similar to the shift seen for other IEM mutations but not previously reported for PEPD mutations, of the midpoint of activation by the A1632E channels of 7 mV in the hyperpolarizing direction (-33.3 ± 0.6 mV for A1632E; -26.2 ± 1.6 mV for WT; $p < 0.001$).
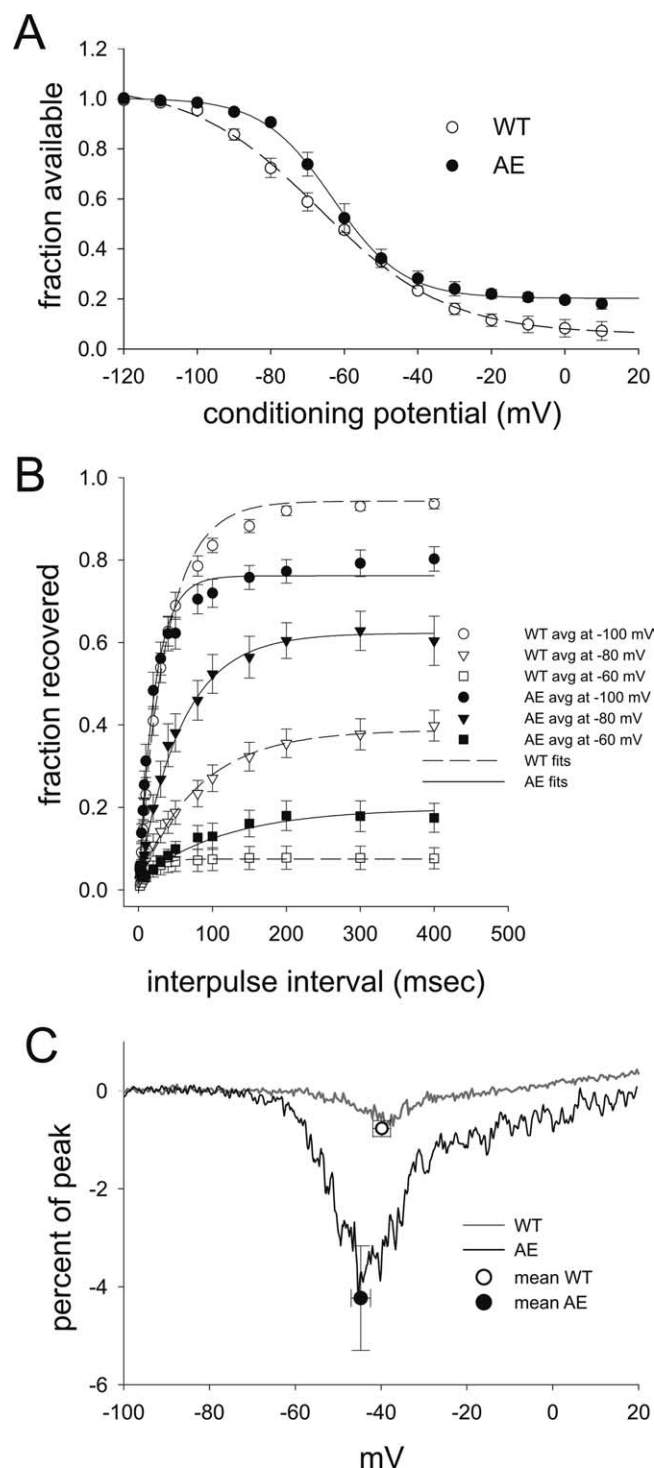
Closer examination of the Boltzmann curves fitted to the averages for the A1632E displayed offsets from zero for both activation and inactivation (Fig. 2E). The offset from zero for activation was unexpected but was probably attributable to the low peak currents in A1632E-expressing cells, because the analysis finds peak inward currents and the offset represents actual currents of only 20–30 pA in reference to 1 nA I_{max}, which was similar to bandwidth noise when using 10 kHz filtering. To display the window current predicted by the overlap of the activation and fast inactivation curves, the offset from zero determined from the fit of the activation G–V data were subtracted from both the activation and fast inactivation curves to account for the effect of small total I_{max} values. Even after this correction, the offset from zero for A1632E fast inactivation appears to reflect an actual fraction of channels that failed to inactivate as demonstrated in Figure 4. The depolarizing shift of fast inactivation and the hyperpolarizing shift of activation for A1632E channels compared with WT channels results in a substantially increased predicted window current (Fig. 2F).

Slow inactivation

Inactivation of Na$_V$1.7 channels occurs with at least two different time courses. In addition to the fast (10–100 ms) inactivation process, there is an additional inactivation process (slow inactivation) that develops over a much longer time frame (1–10 s). To determine whether the A1632E mutation altered the slow-inactivation process, cells were held at a potential between -120 and 10 mV for 30 s to allow full development of both fast and slow inactivation. A 100 ms pulse to -120 mV was used to recover from fast inactivation, followed by a depolarizing pulse to 0 mV to activate the available channels. As illustrated in Figure 3A, the
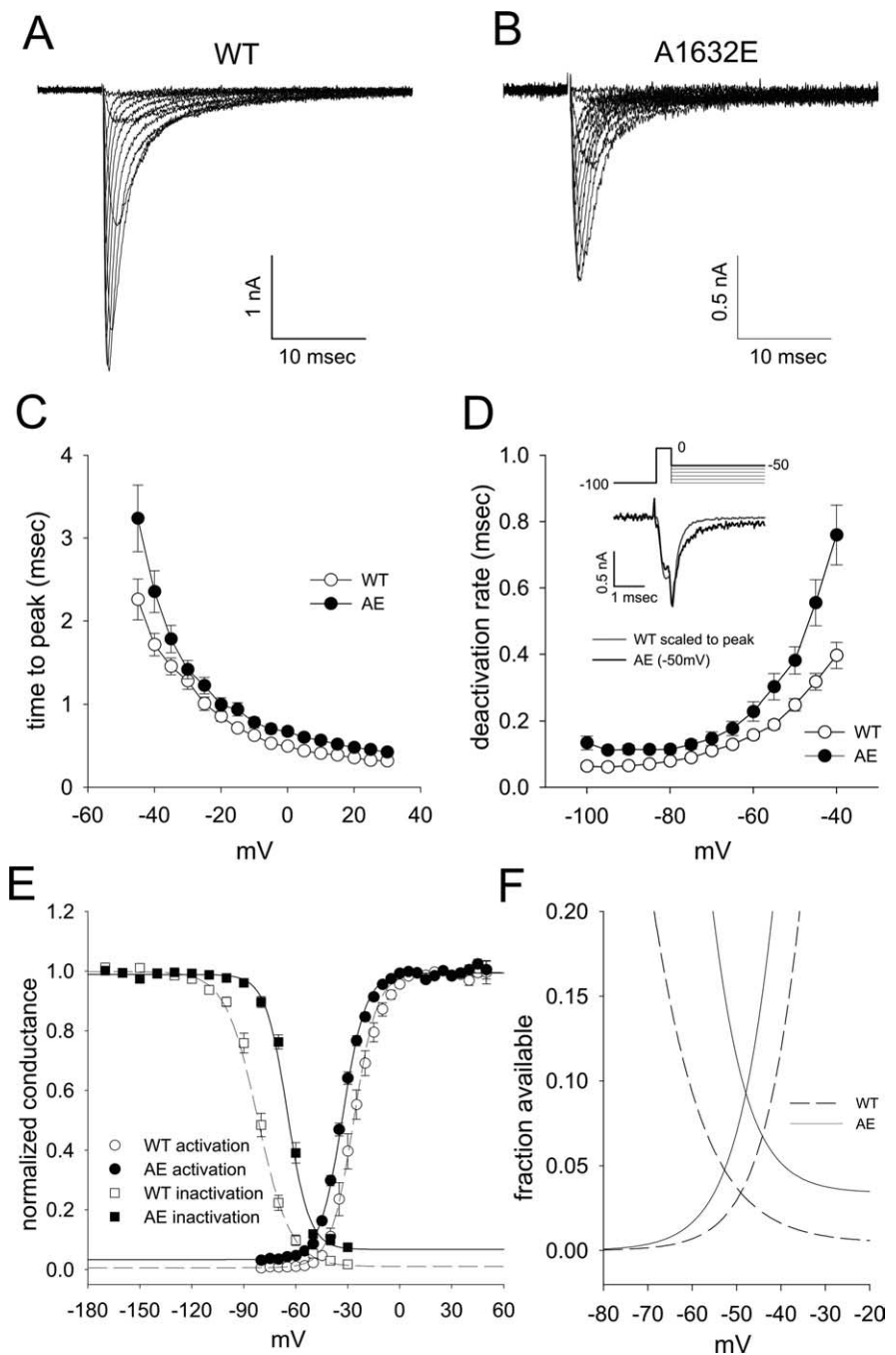
Figure 2. A1632E shifts activation and fast inactivation. ***A***, ***B***, Typical data traces recorded from HEK cell lines expressing either the WT (***A***) or the hNa$_V$1.7r–A1632E mutant (***B***) sodium channel. The current densities from the A1632E-expressing cell line were lower, with total peak inward currents averaging just under 1 nA. In comparison, the hNa$_V$1.7r-WT clone total peak current averaged near 3 nA. For display purposes, the traces were digitally filtered to 2 kHz. ***C***, The average time-to-peak for the traces recorded during the activation protocol are plotted as a function of test potential with the WT ($n = 9$) responses shown by open circles and the A1632E (AE) ($n = 18$) responses are shown by filled circles. Error bars are $\pm$SEM. ***D***, Deactivation kinetics are derived from single-exponential fits to tail currents recorded in response to brief activating pulses (0 mV for 0.5 ms), followed by a repolarization to the indicated potential. Example data traces comparing the deactivation during repolarization to -50 mV are shown in the inset. The time constants are averaged and plotted with the WT ($n = 9$) shown by open circles and the A1632E ($n = 7$) shown by filled circles. Error bars are $\pm$SEM. ***E***, The peak inward currents elicited using either the activation or the fast-inactivation protocol were transformed into normalized conductance as described in Materials and Methods, and the average response at each test voltage was plotted using open symbols for WT ($n = 9$) and filled symbols for A1632E ($n = 18$). The activation data are plotted using circles and the fast-inactivation data are plotted using squares. Error bars are $\pm$SEM. The smooth lines are Boltzmann fits to the average values. The small offset of the activation curve is a result of the small total currents recorded from A1632E-expressing cells so that the peak inward current obtained from the baseline fluctuations represents a few percentage of I_{max}. The baseline offset from the fit of the A1632E inactivation data, however, likely corresponds to an incomplete inactivation resulting in persistent current. ***F***, The predicted window current is larger for A1632E (solid lines) compared with WT (dashed lines).

voltage dependence of slow inactivation for A1632E channels was altered compared with WT channels. Boltzmann fits revealed that, although the midpoint of slow inactivation is similar (-66.7 mV for WT; -63.2 mV for A1632E), the slope was steeper for the A1632E channels compared with WT (-9.56 vs -17.37), and, similar to fast inactivation, there was a fourfold increase in the fraction of channels that appear resistant to the slow inactivation process (0.203 for A1632E vs 0.05 for WT).

Recovery from inactivation

Recovery from inactivation (repriming) occurs at different rates for specific channel subtypes, and the rate and extent of recovery is voltage dependent. This repriming of the channels was measured using a two-pulse protocol and varying the interpulse interval as well as the interpulse potential. The cell was first pulsed to 0 mV for 20 ms to allow complete fast inactivation and then repolarized to a specified potential for a range of durations to allow channel recovery, which is quantified as the ratio of the current evoked by the second pulse to 0 mV compared with the response to the first pulse. The rate and extent of recovery, comparing A1632E and WT channels for three different interpulse potentials, are shown in Figure 3B. At hyperpolarized interpulse potentials such as shown for -100 mV, the rate of recovery was rapid and was similar between A1632E and WT channels. For interpulse potentials of -80 and -60 mV, however, both the rate and the fraction of current recovered were larger for A1632E channels compared with WT channels.

Persistent currents

For both the fast inactivation and the slow inactivation protocols, the A1632E channels exhibited a fraction of channels resistant to inactivation. Non-inactivating channels could result in persistent sodium currents. The fraction of persistent current seen from A1632E-expressing cells was evaluated in two ways, by determining the offsets after fitting inactivation with an exponential function or by comparing the current that persists at 100 ms after onset of depolarization. The inactivation decay from A1632E cells, obtained by fitting with a single-exponential function, consistently needed an offset constant. The rate of fast inactivation as a function of stimulus pulse potential is shown in Figure 4A, which shows that the kinetics of A1632E channels are significantly slowed over the voltage range between -25 and $+35$ mV. Examples of traces showing the difference in inactivation between WT and A1632E currents and the persistent current at 100 ms are shown in Figure 4B–D. With pulses to -20 mV, which was near the voltage for peak current, the A1632E current decayed more slowly than WT and did not decay to zero. The same two traces at the end of the depolarization pulse are displayed at

Figure 3. A1632E mutation effects slow-inactivation, repriming, and slow ramp currents. *A*, The slow-inactivation protocol consists of a 30 s conditioning pulse, followed by a 100 ms pulse to -120 mV to restore the fast-inactivation state and then pulsed to 0 mV for 50 ms to activate the fraction of available channels. The A1632E data (filled circles; $n = 5$) show greater availability at all potentials compared with wild-type (open circles; $n = 5$) with the difference being greatest in the voltage range of -90 to -70 mV. In addition, there is a more prominent fraction of channels that do not become slow inactivated at the potentials more positive to -20 mV. The smooth lines are Boltzmann fits with the following parameters: WT: $I_{max} = 0.99$, $I_{min} = 0.058$, $V_{1/2} = -66.7$ mV, and $k = 17.4$; A1632E: $I_{max} = 1.0$, $I_{min} = 0.2$, $V_{1/2} = -63.2$ mV, and $k = 9.5$. *B*, The A1632E mutation alters recovery from fast inactivation. From a holding potential of -100 mV, fast inactivation was initiated by a step to 0 mV for 20 ms, followed by a hyperpolarizing step to a recovery potential that varied in time (2–400 ms) and amplitude (-100 to -60 mV). The recovery period was followed by a second depolarizing test pulse to 0 mV. For each recovery potential, the peak inward current in response to the test pulse was

normalized by the amplitude of the response to the inactivation step and plotted as a function of recovery period duration. The averages for cells expressing WT channels (open symbols; $n = 7$) and A1632E channels (filled symbols; $n = 8$) are shown with error bars $\pm$SEM. Single-exponential functions were fit to these averaged data and are shown by solid lines for A1632E and dashed lines for WT. *C*, This panel illustrates the responses to a ramp pulse protocol that spans the range of -100 to 20 mV over 600 ms (0.2 mV/ms). The response has been rescaled as the percentage of peak inward current recorded during the activation *I–V* protocol. The peak currents from wild-type hNa$_V$1.7 are much larger than from the A1632E-expressing cells, thus scaling the noise to be quieter. In addition, for display purposes, the WT trace has been post-acquisition filtered to 1 kHz, and the A1632E trace has been post-acquisition filtered to 500 Hz. The average peak ramp current from the A1632E cells was $4.2 \pm 0.3\%$ at -44.7 ± 0.7 mV ($n = 12$), whereas the peak ramp current from the WT cells averaged $0.77 \pm 0.05\%$ at -39.8 ± 0.7 mV ($n = 9$). Error bars are 1 SD.

higher gain in the inset, which clearly shows that the A1632E current has persisted for at least 100 ms (Fig. 4B). With pulses to +15 mV, whereas the inactivation rate for WT channels has continued to speed up, the inactivation rate for A1632E channels appears to have leveled off (Fig. 4C); the inset shows that, even at this potential, the A1632E current has persisted for at least 100 ms. If the A1632E channels exhibit persistent currents in the subthreshold range, this could contribute to neuronal hyperexcitability. Figure 4D shows the response of WT and A1632E channels to a pulse to −50 mV, and once again the inset shows that A1632E current persists to at least 100 ms.
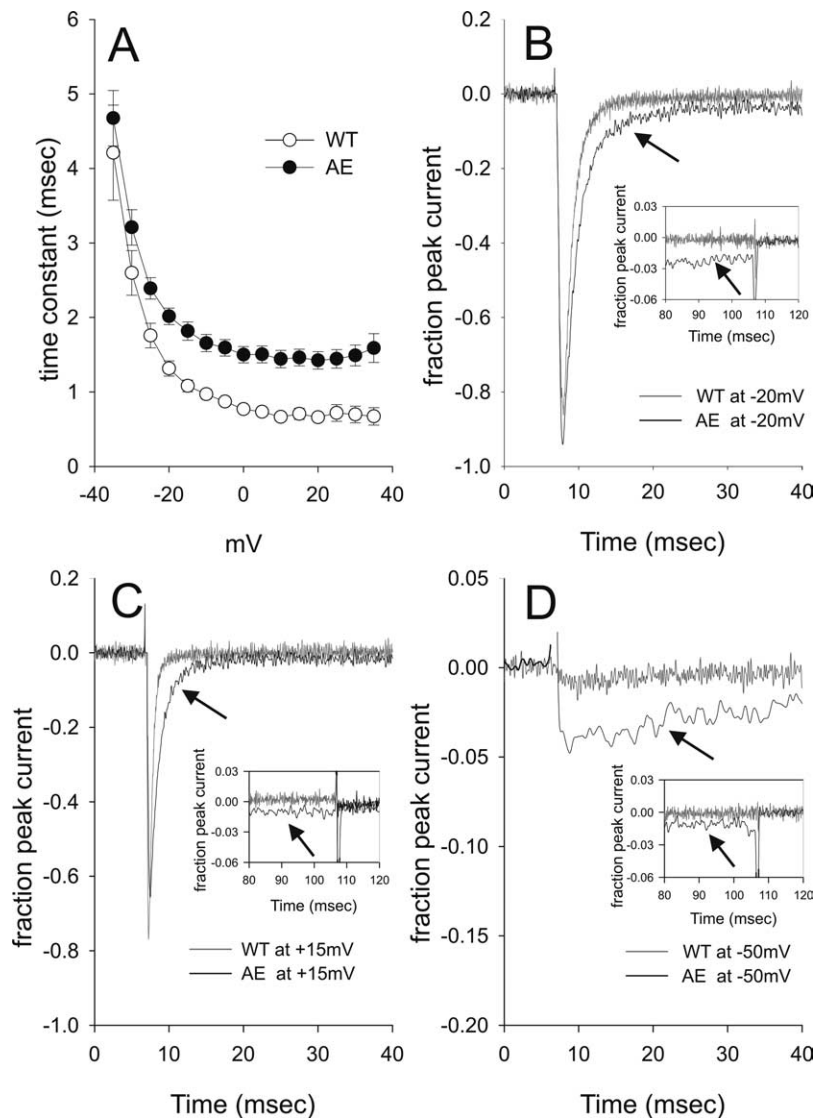
Quantification of the A1632E persistent current can be achieved by either fitting exponential functions or measuring the mean current for a 10 ms window near the end of the 100 ms activation pulse. Using either method, the peak persistent current averaged ∼4% of the peak current from the I–V curve for each A1632E cell.

Ramp responses

We evaluated the response of WT and A1632E channels to small slow depolarizations using a slow ramp protocol that starts from a holding potential of −100 mV and steadily increases the applied potential to +20 mV over 600 ms for a ramp rate of 0.2 mV/ms. This slow rate fully inactivates many voltage-gated sodium channels, but Na$_V$1.7 and many disease-causing Na$_V$1.7 mutations still respond to this protocol. To compare between cells, the response is normalized to the peak inward current recorded during the activation I–V protocol. The response of the A1632E mutant compared with WT channels is shown in Figure 3C. The peak of the slow ramp response of A1632E-expressing cells averaged 4.2%, which is a fivefold increase over the average ramp response of 0.77% in WT-expressing cells. In addition, the slow ramp response from A1632E-expressing cells typically showed a shoulder after the peak response that is consistent with a small fraction of channels persistently staying open.


Figure 4. Fast inactivation is slowed and incomplete in A1632E-expressing cells. **A**, The decaying phase of the inward sodium current elicited by the activation protocol was fit to a single-exponential for the voltage range of −35 to +35 mV. The average time constant is plotted as a function of voltage for WT cells (open circles; n = 8) and for A1632E cells (filled circles; n = 18) Error bars are ±SEM. **B**, Example traces elicited by pulses to −20 mV are shown superimposed and normalized to peak inward current to illustrate the difference in inactivation rate between WT-expressing (gray line) and A1632E-expressing (black line, arrow) cells. The end of the 100 ms trace (which was cutoff in the main panel to illustrate kinetics) is shown as an inset with an expanded vertical axis to show that A1632E current (black line, arrow) persists for at least 100 ms. **C**, Example traces elicited by pulses to +15 mV are superimposed and normalized to peak inward current to illustrate the greater difference in inactivation rate at this depolarized potential. The inset shows that, even at this depolarized potential, persistent current can still be resolved from A1632E cells. **D**, Example traces elicited by pulses to −50 mV (nearer to RMP range and near threshold for voltage activation) are superimposed and normalized to peak inward current to illustrate that persistent current is resolvable in this voltage range (inset, black line, arrow). Note the expanded scale in **D**. For display purposes, the WT traces were digitally filtered to 2 kHz in the main panels and filtered to 1 kHz in the insets, whereas the A1632E traces were digitally filtered to 1 kHz in the main panels of **B** and **C** and filtered to 500 Hz in **D** and all insets.

Current-clamp recordings: DRG neurons

To assess the effect of the A1632E mutation on excitability, DRG neurons were transfected with either the WT or A1632E construct, and current-clamp recording conditions were used to determine RMP, action potential threshold, and firing frequency in small (22–28 μm) DRG neurons. The average size of the recorded DRG neurons was 25.4 ± 0.2 μm (n = 30) for WT-transfected and 25.3 ± 0.4 μm (n = 28) for A1632E-transfected cells. The RMP was −56.8 ± 1.1 mV for WT cells and was −54.2 ± 2.7 mV for A1632E cells. This small depolarization of A1632E RMP was

not statistically significant. The input resistance was also similar between groups (719 ± 71 MΩ for WT; 695 ± 90 MΩ for A1632E). The main difference between these two groups was a reduction of current threshold for single action potentials for the A1632E-transfected cells (200 ± 36 pA for WT; 132 ± 22 pA for A1632E; $p < 0.05$).

The firing of action potentials of a representative DRG neuron transfected with either WT or A1632E is shown at threshold current stimuli (Fig. 5A,B) and at current injections (1 s duration) near two and three times threshold as well as the current injection
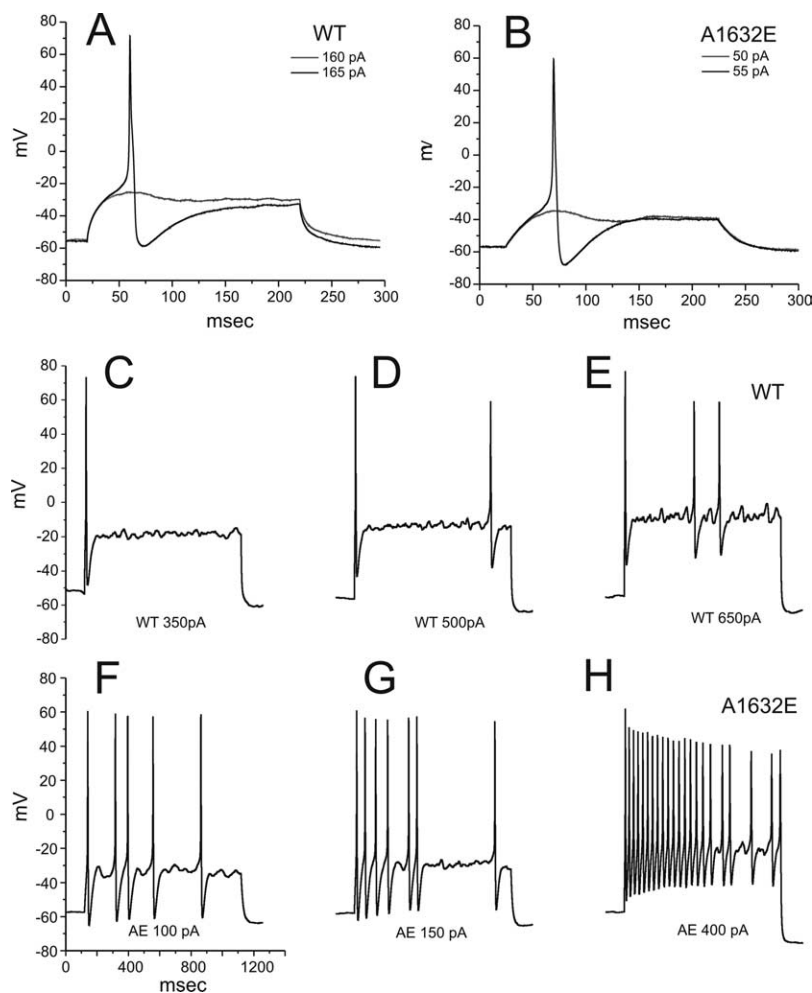
Figure 5. Current-clamp recordings in transfected DRG neurons. The A1632E mutation decreases action potential threshold in small, current-clamped DRG neurons. ***A***, Responses of a current-clamped DRG neuron transfected with hNa$_V$1.7r–WT DNA to a series of subthreshold and suprathreshold depolarizing current stimuli stepped in 5 pA increments. Two traces are displayed that show the threshold value for eliciting an action potential. RMP for this cell was −56 mV and threshold was 165 pA. ***B***, Two traces are displayed that show the threshold value for a DRG neuron transfected with hNa$_V$1.7r–A1632E DNA. RMP for this cell was −57 mV and threshold was 55 pA. Example action potential responses from DRG neurons transfected with hNa$_V$1.7r–WT and hNa$_V$1.7r–A1632E DNA. ***C–E*** illustrate the responses elicited at currents approximately two and three times threshold as well as the stimuli that elicited the maximal response for DRG neurons transfected with hNa$_V$1.7r–WT DNA. ***F–H*** show the responses for DGR neurons transfected with hNa$_V$1.7r–A1632E DNA. These cells are the same as shown in ***A*** and ***B*** to determine action potential threshold.

that elicited the maximal number of action potentials (Fig. 5C–H). At threshold, there was no difference in either the average action potential peak depolarization (58.8 ± 1.8 mV for WT; 54.6 ± 2.8 mV for A1632E) or the peak afterhyperpolarization (AHP) (−63 ± 1.6 mV for WT; −63 ± 1.5 mV for A1632E). Figure 5, C–E, shows representative WT-transfected DRG neurons that produce mostly single action potentials in response to a 1 s depolarization with an occasional second or third spike elicited by strong stimuli. A1632E-transfected DRG neurons, in contrast, commonly generated multiple action potentials. To compare the responses of DRG neurons transfected with either WT or A1632E sodium channels, the number of spikes elicited for current injections ranging from 50 to 500 pA in 50 pA steps were averaged together and plotted in Figure 6A. For each stimulus level, the A1632E-transfected DRG neurons responded with significantly more spikes compared with WT.

Current-clamp recording: trigeminal ganglion neurons

The A1632E mutation was found in a patient whose clinical phenotype includes pain in the periocular and mandibular regions of the face. Because these areas are innervated by sensory neurons that reside in the trigeminal ganglion, we asked whether the A1632E mutation would induce hyperexcitability in those neurons. To assess the effect of the A1632E mutation on excitability, current-clamp recording was used to determine RMP, action potential threshold, and firing frequency in small (22–28 μm) rat trigeminal ganglion neurons that were transfected with either the WT or A1632E construct. The average size of the recorded trigeminal ganglion neurons was 23.8 ± 0.5 μm (n = 27) for WT-transfected cells and 24.4 ± 0.5 μm (n = 27) for A1632E. The RMP was −52.8 ± 1.5 mV for WT cells and −52.9 ± 1.5 mV for A1632E cells. The only significant difference was for input resistance (720 ± 102 MΩ for WT; 516 ± 26 MΩ for A1632E; $p < 0.05$). There was a trend toward reduction of current threshold for the A1632E-transfected cells (166 ± 21 pA for WT; 144 ± 24 pA for A1632E), but it did not reach statistical significance.

Similar to DRG neurons, representative trigeminal ganglion neurons transfected with either WT or A1632E channels are shown to illustrate the response at threshold (Fig. 7A,B) as well as the response to current injections near two and three times threshold and to stimuli eliciting the maximal response (Fig. 7C–H). At threshold, there was no difference in either the average action potential peak depolarization (55.2 ± 3.0 mV for WT; 55.8 ± 2.5 mV for A1632E) or the peak AHP (−58.2 ± 1.6 mV for WT; −59.9 ± 1.0 mV for A1632E). As shown in Figure 6B, trigeminal ganglion neurons transfected with A1632E responded with more spikes than neurons transfected with WT as measured at each stimulus level.

Discussion

In this study, we have identified a new mutation (A1632E) of the Na$_V$1.7 sodium channel in a patient with a painful disorder that includes clinical characteristics of both IEM and PEPD. Previously described IEM mutations all shift activation in a hyperpolarizing direction and slow deactivation, and many of these mutations enhance the Na$_V$1.7 ramp current (Dib-Hajj et al., 2007). Computer simulations suggest that the shift in activation is the largest contributor to DRG neuron hyperexcitability (Sheets et al., 2007). In contrast, previously described PEPD mutations of Na$_V$1.7 impair inactivation but have not been described as affecting activation or deactivation (Fertleman et al., 2006; Jarecki et al., 2008). We show here that the A1632E mutation has a mixed

A

B
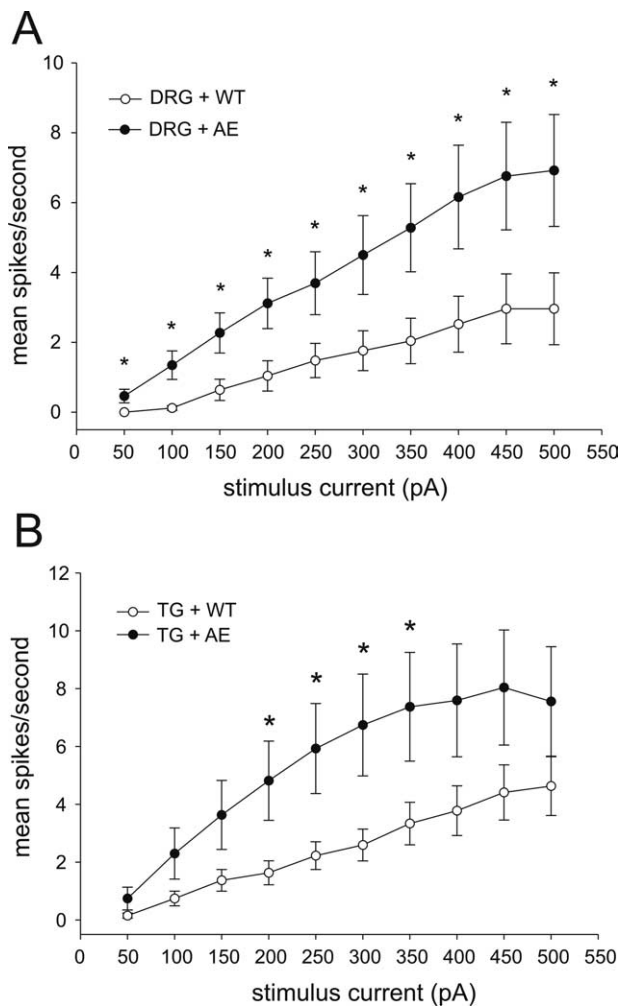
Figure 6. A1632E expression increases excitability in DRG and trigeminal ganglion neurons. The mean number of action potentials (defined as action potentials that overshoot 0 mV) is quantified in response to a series of 1-s-long current injections ranging from 50 to 500 pA in 50 pA increments. **A**, The mean response was significantly higher ($p < 0.05$) for DRG neurons transfected with $hNa_V1.7r$–A1632E (AE) ($n = 28$) compared with WT ($n = 30$) at every stimulus level. Error bars are $\pm$ SEM. **B**, The mean response reached significance ($p < 0.05$) for trigeminal ganglion neurons (TG) transfected with $hNa_V1.7r$–A1632E ($n = 27$) compared with WT ($n = 27$) for current injections between 200 and 350 pA. Error bars are $\pm$ SEM.

physiological profile, with properties characteristic of both IEM and PEPD mutations. Using voltage-clamp recordings, we demonstrate that A1632E impairs fast inactivation, which is shifted 17 mV in a depolarizing direction, and slows fast inactivation, which is incomplete, resulting in persistent inward currents. We also demonstrate that A1632E produces a 7 mV hyperpolarizing shift in activation, slows deactivation, accelerates repriming, and increases the depolarizing response to slow ramp stimuli. Using current clamp, we demonstrate that A1632E increases the frequency of firing in response to suprathreshold stimuli, in both DRG and trigeminal ganglion neurons.

The length and sequence of the S4–S5 linker in domain IV, which carries the A1632E mutation, are highly conserved among most sodium channels described to date, suggesting an important role in normal channel function. Indeed, $Na_V1.4$ channels with small insertions at two sites in this linker do not generate sodium currents (Mitrovic et al., 1996). Mutations in this linker have been identified in $Na_V1.1$ from patients with severe myoclonic epilepsy of infancy (Claes et al., 2003; Nabbout et al., 2003), in

$Na_V1.4$ with diseases of skeletal muscle (Mitrovic et al., 1996; Fleischhauer et al., 1998; Rossignol et al., 2007; Schoser et al., 2007), and in $Na_V1.5$ with cardiac disorders (Ruan et al., 2007). It is noteworthy that the A1632E mutation in $Na_V1.7$ in this child with a chronic pain disorder is analogous to the A1481D mutation in $Na_V1.4$ reported with cold-aggravated myotonia (Schoser et al., 2007). It remains to be seen whether the effects of A1481D on gating properties of $Na_V1.4$ are similar to the effects of A1632E on $Na_V1.7$.

The A1632E mutation is located within the DIV/S4–S5 linker, close to the PEPD mutation M1627K (Fertleman et al., 2006), suggesting a possible explanation for the effect of A1632E on $Na_V1.7$ gating properties. Although a large shift of fast-inactivation voltage dependence is produced by both M1627K (Fertleman et al., 2006; Dib-Hajj et al., 2008) and A1632E (this study), the impairment of inactivation is smaller than with I1461T and T1464I PEPD mutations of the IFMT inactivation particle, which show a more substantial non-inactivating (persistent) inward current (Fertleman et al., 2006). Why the M1627K and A1632E mutations are better tolerated is not yet understood. The possibility that these mutations influence S4–S5 linker folding and therefore affect inactivation (Tang et al., 1996; Lerche et al., 1997; Smith and Goldin, 1997; McPhee et al., 1998) merits additional study.

An alanine residue is conserved at the site corresponding to A1632 in all sodium channels except $Na_V1.9$, a channel characterized by hyperpolarized voltage dependence of activation and very slow inactivation, causing a persistent current (Cummins et al., 1999; Dib-Hajj et al., 1999), in which it is replaced by a serine (Fig. 1). It is possible that substitution of a serine for alanine in the DIV/S4–S5 linker contributes to these properties of $Na_V1.9$. Surprisingly, a double mutation in $Na_V1.5$ (P1655Q/A1656Q), which includes the site analogous to A1632 in $Na_V1.7$, had no effect on the activation voltage dependence or the kinetics of inactivation but shifted inactivation in a hyperpolarized direction (Tang et al., 1998). However, it is difficult to assess the contribution of this residue to the gating properties of $Na_V1.5$, because the single A1656Q mutation was not studied. A1632S substitution in $Na_V1.7$, which recapitulates the sequence of this linker in $Na_V1.9$, does not induce major shifts in activation or inactivation as seen with A1632E (data not shown). This suggests that a serine is better tolerated than a glutamate at this position. The mutant phenotype may be caused by the presence of a charge that destabilizes the inactivation complex, biasing the channel toward the activated/open state.

PEPD and IEM display distinct clinical phenotypes, with PEPD characterized by paroxysmal pain in a rectal, periocular, and perimandibular distribution, and IEM characterized by pain in the feet and, in most cases, the hands. Previously described PEPD mutations have been shown to impair inactivation and have not been reported to affect activation or deactivation (Fertleman et al., 2006; Jarecki et al., 2008). In contrast, mutations linked to IEM have been observed to hyperpolarize activation and slow deactivation, either without an effect on inactivation (Cummins et al., 2004; Choi et al., 2006; Lampert et al., 2006; Sheets et al., 2007; Cheng et al., 2008) or coupled to a shift in inactivation voltage dependence, which was, nevertheless, complete (Dib-Hajj et al., 2005; Han et al., 2006; Harty et al., 2006). The shifts of voltage dependence of activation and fast inactivation for these PEPD and IEM mutants are illustrated in Figure 8. The PEPD and IEM mutations characterized to date exhibit distinct nonoverlapping groupings of electrophysiological proper-
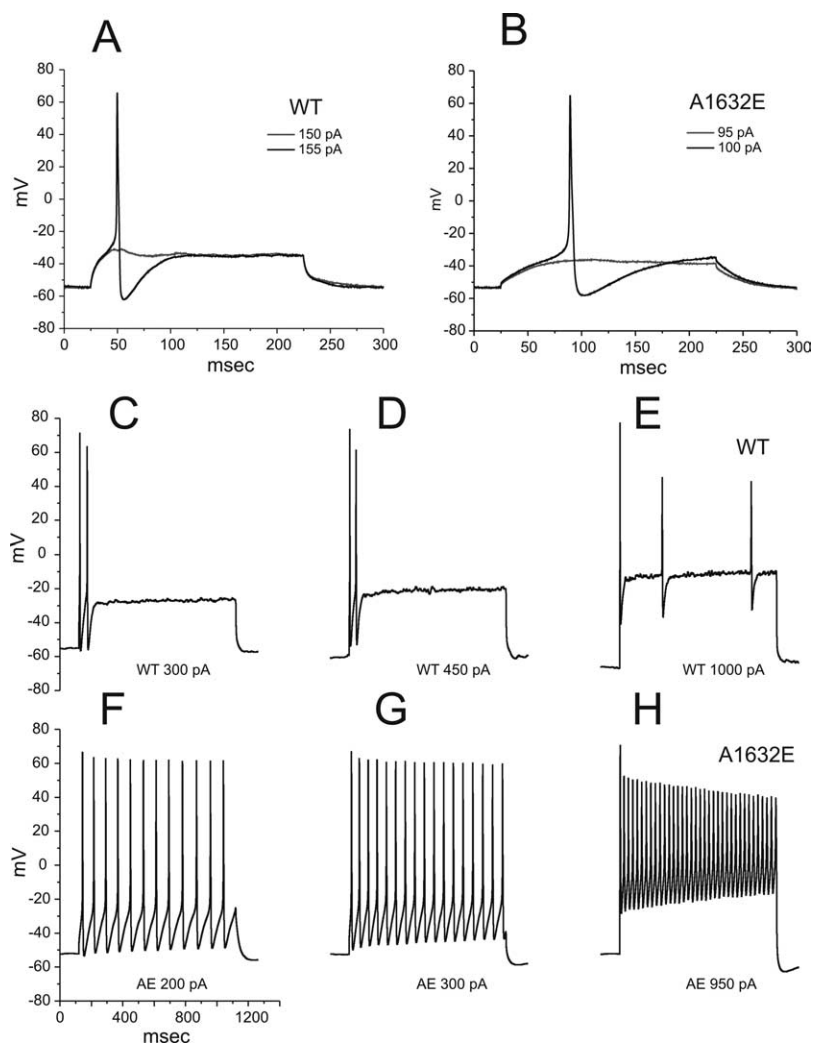
Figure 7. Current-clamp recordings from transfected trigeminal ganglion neurons. The A1632E mutation decreases action potential threshold in small, current-clamped trigeminal ganglion neurons. ***A***, Responses of a current-clamped trigeminal neuron transfected with hNa$_V$1.7r–WT DNA to a series of subthreshold and suprathreshold depolarizing current stimuli stepped in 5 pA increments. Two traces are displayed that show the threshold value for eliciting an action potential. RMP for this cell was −54 mV and threshold was 155 pA. ***B***, Two traces are displayed that show the threshold for a trigeminal neuron transfected with hNa$_V$1.7r–A1632E DNA. RMP for this cell was −54 mV and threshold was 100 pA. ***C–E*** illustrate the responses elicited at currents approximately two and three times threshold as well as the response to a stimulus that elicited the maximal response for trigeminal neurons transfected with hNa$_V$1.7r–WT DNA. ***F–H*** show the responses for trigeminal neurons transfected with hNa$_V$1.7r–A1632E DNA. These cells are the same as shown in ***A*** and ***B*** to determine action potential threshold.

ties that correlate to and possibly predict their clinical phenotypes.

The A1632E mutation is associated with a mixed clinical phenotype that includes features of both PEPD (pain in perirectal, perimandibular, and periorbital areas) and erythromelalgia (pain in feet and hands). In parallel, A1632E exhibits a functional profile that includes electrophysiological properties characteristic of both PEPD and IEM (Fig. 8). As illustrated in this figure, comparison of the previously published IEM and PEPD mutations suggests that hyperpolarizing shifts in activation produce IEM, whereas depolarizing shifts in fast inactivation produce PEPD. The A1632E mutant provides evidence, in humans, that a Na$_V$1.7 mutation causing both a hyperpolarizing shift in activation and a depolarizing shift in fast inactivation produces a clinical phenotype with characteristics of both disorders. The present results indicate that IEM and PEPD mutations are part of a physiological

continuum that can produce a continuum of clinical phenotypes, including IEM, overlap disorders, and PEPD.

References

Ahmad S, Dahllund L, Eriksson AB, Hellgren D, Karlsson U, Lund PE, Meijer IA, Meury L, Mills T, Moody A, Morinville A, Morten J, O'Donnell D, Raynoschek C, Salter H, Rouleau GA, Krupp JJ (2007) A stop codon mutation in SCN9A causes lack of pain sensation. Hum Mol Genet 16:2114–2121.

Catterall WA, Goldin AL, Waxman SG (2005) International Union of Pharmacology. XLVII. Nomenclature and structure-function relationships of voltage-gated sodium channels. Pharmacol Rev 57:397–409.

Cheng X, Dib-Hajj SD, Tyrrell L, Waxman SG (2008) Mutation I136V alters electrophysiological properties of the NaV1.7 channel in a family with onset of erythromelalgia in the second decade. Mol Pain 4:1.

Choi JS, Dib-Hajj SD, Waxman SG (2006) Inherited erythermalgia: limb pain from an S4 charge-neutral Na channelopathy. Neurology 67:1563–1567.

Claes L, Ceulemans B, Audenaert D, Smets K, Löfgren A, Del-Favero J, Ala-Mello S, Basel-Vanagaite L, Plecko B, Raskin S, Thiry P, Wolf NI, Van Broeckhoven C, De Jonghe P (2003) De novo SCN1A mutations are a major cause of severe myoclonic epilepsy of infancy. Hum Mutat 21:615–621.

Cox JJ, Reimann F, Nicholas AK, Thornton G, Roberts E, Springell K, Karbani G, Jafri H, Mannan J, Raashid Y, Al-Gazali L, Hamamy H, Valente EM, Gorman S, Williams R, McHale DP, Wood JN, Gribble FM, Woods CG (2006) An SCN9A channelopathy causes congenital inability to experience pain. Nature 444:894–898.

Cummins TR, Howe JR, Waxman SG (1998) Slow closed-state inactivation: a novel mechanism underlying ramp currents in cells expressing the hNE/PN1 sodium channel. J Neurosci 18:9607–9619.

Cummins TR, Dib-Hajj SD, Black JA, Akopian AN, Wood JN, Waxman SG (1999) A novel persistent tetrodotoxin-resistant sodium current in SNS-null and wild-type small primary sensory neurons. J Neurosci 19:RC43(1–6).

Cummins TR, Dib-Hajj SD, Waxman SG (2004) Electrophysiological properties of mutant Nav1.7 sodium channels in a painful inherited neuropathy. J Neurosci 24:8232–8236.

Dib-Hajj SD, Tyrrell L, Black JA, Waxman SG (1998) NaN, a novel voltage-gated Na channel, is expressed preferentially in peripheral sensory neurons and down-regulated after axotomy. Proc Natl Acad Sci U S A 95:8963–8968.

Dib-Hajj SD, Tyrrell L, Cummins TR, Black JA, Wood PM, Waxman SG (1999) Two tetrodotoxin-resistant sodium channels in human dorsal root ganglion neurons. FEBS Lett 462:117–120.

Dib-Hajj SD, Rush AM, Cummins TR, Hisama FM, Novella S, Tyrrell L, Marshall L, Waxman SG (2005) Gain-of-function mutation in Nav1.7 in familial erythromelalgia induces bursting of sensory neurons. Brain 128:1847–1854.

Dib-Hajj SD, Cummins TR, Black JA, Waxman SG (2007) From genes to pain: Na v 1.7 and human pain disorders. Trends Neurosci 30:555–563.

Dib-Hajj SD, Estacion M, Jarecki BW, Tyrrell L, Fisher TZ, Lawden M, Cummins TR, Waxman SG (2008) Paroxysmal extreme pain disorder M1627K mutations in human Nav1.7 renders DRG neurons hyperexcitable. Mol Pain 4:37.

Djouhri L, Newton R, Levinson SR, Berry CM, Carruthers B, Lawson SN
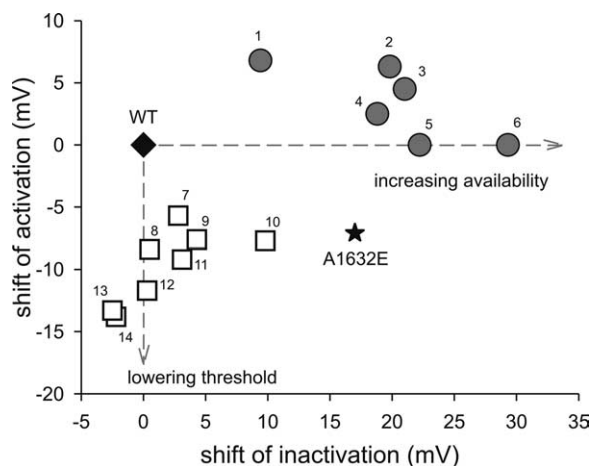
Figure 8. Comparison of IEM and PEPD mutations. The shifts in the voltage dependence of activation and fast inactivation of each mutant compared with wild-type hNa$_V$1.7 are plotted with IEM mutants (open squares) and PEPD mutants (gray circles) numbered to identify the specific mutation and reference from which the data were compiled. The WT control is plotted as a black diamond at (0,0). The dotted lines through (0,0) demarcate between positive and negative shifts and indicate the outcome for the shifts. The A1632E mutation is plotted with the star symbol and shows shifts in activation and inactivation common to both IEM and PEPD mutants. The identity of each numbered symbol is as follows: 1, T1464I (Fertleman et al., 2006); 2, V1298F (Jarecki et al., 2008); 3, V1299F (Jarecki et al., 2008); 4, I1461T (Jarecki et al., 2008); 5, M1627K (Fertleman, 2006); 6, I1461T (Fertleman, 2006); 7, I136V (Cheng et al., 2008); 8, S241T (Lampert et al., 2006); 9, F1449V (Dib-Hajj, 2005); 10, A863P (Harty et al., 2006); 11, L858F (Han et al., 2006); 12, F216S (Choi et al., 2006); 13, L858H (Cummins et al., 2004); and 14, I848T (Cummins et al., 2004).

(2003) Sensory and electrophysiological properties of guinea-pig sensory neurones expressing Nav 1.7 (PN1) Na$^+$ channel alpha subunit protein. J Physiol 546:565–576.

Drenth JP, Waxman SG (2007) Mutations in sodium-channel gene SCN9A cause a spectrum of human genetic pain disorders. J Clin Invest 117:3603–3609.

Drenth JP, te Morsche RH, Guillet G, Taieb A, Kirby RL, Jansen JB (2005) SCN9A mutations define primary erythermalgia as a neuropathic disorder of voltage gated sodium channels. J Invest Dermatol 124:1333–1338.

Felts PA, Yokoyama S, Dib-Hajj S, Black JA, Waxman SG (1997) Sodium channel alpha-subunit mRNAs I, II, III, NaG, Na6 and hNE (PN1): different expression patterns in developing rat nervous system. Brain Res Mol Brain Res 45:71–82.

Fertleman CR, Baker MD, Parker KA, Moffatt S, Elmslie FV, Abrahamsen B, Ostman J, Klugbauer N, Wood JN, Gardiner RM, Rees M (2006) SCN9A mutations in paroxysmal extreme pain disorder: allelic variants underlie distinct channel defects and phenotypes. Neuron 52:767–774.

Fleischhauer R, Mitrovic N, Deymeer F, Lehmann-Horn F, Lerche H (1998) Effects of temperature and mexiletine on the F1473S Na+ channel mutation causing paramyotonia congenita. Pflugers Arch 436:757–765.

Goldberg Y, MacFarlane J, MacDonald ML, Thompson J, Dube MP, Mattice M, Fraser R, Young C, Hossain S, Pape T, Payne B, Radomski C, Donaldson G, Ives E, Cox J, Younghusband HB, Green R, Duff A, Boltshauser E, Grinspan GA, Dimon JH, et al. (2007) Loss-of-function mutations in the Nav1.7 gene underlie congenital indifference to pain in multiple human populations. Clin Genet 71:311–319.

Han C, Rush AM, Dib-Hajj SD, Li S, Xu Z, Wang Y, Tyrrell L, Wang X, Yang Y, Waxman SG (2006) Sporadic onset of erythermalgia: a gain-of-function mutation in Nav1.7. Ann Neurol 59:553–558.

Harty TP, Dib-Hajj SD, Tyrrell L, Blackman R, Hisama FM, Rose JB, Waxman SG (2006) Na$_V$1.7 mutant A863P in erythromelalgia: effects of altered activation and steady-state inactivation on excitability of nociceptive dorsal root ganglion neurons. J Neurosci 26:12566–12575.

Herzog RI, Cummins TR, Ghassemi F, Dib-Hajj SD, Waxman SG (2003) Distinct repriming and closed-state inactivation kinetics of Nav1.6 and Nav1.7 sodium channels in mouse spinal sensory neurons. J Physiol 551:741–750.

Jarecki BW, Sheets PL, Jackson JO 2nd, Cummins TR (2008) Paroxysmal ex-

treme pain disorder mutations within the D3/S4–S5 linker of Nav1.7 cause moderate destabilization of fast-inactivation. J Physiol 586:4137–4153.

Klugbauer N, Lacinova L, Flockerzi V, Hofmann F (1995) Structure and functional expression of a new member of the tetrodotoxin-sensitive voltage-activated sodium channel family from human neuroendocrine cells. EMBO J 14:1084–1090.

Lampert A, Dib-Hajj SD, Tyrrell L, Waxman SG (2006) Size matters: erythromelalgia mutation S241T in Nav1.7 alters channel gating. J Biol Chem 281:36029–36035.

Lee MJ, Yu HS, Hsieh ST, Stephenson DA, Lu CJ, Yang CC (2007) Characterization of a familial case with primary erythromelalgia from Taiwan. J Neurol 254:210–214.

Lerche H, Peter W, Fleischhauer R, Pika-Hartlaub U, Malina T, Mitrovic N, Lehmann-Horn F (1997) Role in fast inactivation of the IV/S4–S5 loop of the human muscle Na$^+$ channel probed by cysteine mutagenesis. J Physiol 505:345–352.

McPhee JC, Ragsdale DS, Scheuer T, Catterall WA (1998) A critical role for the S4–S5 intracellular loop in domain IV of the sodium channel alpha-subunit in fast inactivation. J Biol Chem 273:1121–1129.

Michiels JJ, te Morsche RH, Jansen JB, Drenth JP (2005) Autosomal dominant erythermalgia associated with a novel mutation in the voltage-gated sodium channel alpha subunit Nav1.7. Arch Neurol 62:1587–1590.

Mitrovic N, Lerche H, Heine R, Fleischhauer R, Pika-Hartlaub U, Hartlaub U, George AL Jr, Lehmann-Horn F (1996) Role in fast inactivation of conserved amino acids in the IV/S4–S5 loop of the human muscle Na$^+$ channel. Neurosci Lett 214:9–12.

Nabbout R, Gennaro E, Dalla Bernardina B, Dulac O, Madia F, Bertini E, Capovilla G, Chiron C, Cristofori G, Elia M, Fontana E, Gaggero R, Granata T, Guerrini R, Loi M, La Selva L, Lispi ML, Matricardi A, Romeo A, Tzolas V, Valseriati D, et al. (2003) Spectrum of SCN1A mutations in severe myoclonic epilepsy of infancy. Neurology 60:1961–1967.

Rossignol E, Mathieu J, Thiffault I, Tétreault M, Dicaire MJ, Christian N, Dupré N, Puymirat J, Brais B (2007) A novel founder SCN4A mutation causes painful cold-induced myotonia in French-Canadians. Neurology 69:1937–1941.

Ruan Y, Liu N, Bloise R, Napolitano C, Priori SG (2007) Gating properties of SCN5A mutations and the response to mexiletine in long-QT syndrome type 3 patients. Circulation 116:1137–1144.

Rush AM, Cummins TR, Waxman SG (2007) Multiple sodium channels and their roles in electrogenesis within dorsal root ganglion neurons. J Physiol 579:1–14.

Sangameswaran L, Fish LM, Koch BD, Rabert DK, Delgado SG, Ilnicka M, Jakeman LB, Novakovic S, Wong K, Sze P, Tzoumaka E, Stewart GR, Herman RC, Chan H, Eglen RM, Hunter JC (1997) A novel tetrodotoxin-sensitive, voltage-gated sodium channel expressed in rat and human dorsal root ganglia. J Biol Chem 272:14805–14809.

Schoser BG, Schröder JM, Grimm T, Sternberg D, Kress W (2007) A large German kindred with cold-aggravated myotonia and a heterozygous A1481D mutation in the SCN4A gene. Muscle Nerve 35:599–606.

Sheets PL, Jackson JO 2nd, Waxman SG, Dib-Hajj SD, Cummins TR (2007) A Nav1.7 channel mutation associated with hereditary erythromelalgia contributes to neuronal hyperexcitability and displays reduced lidocaine sensitivity. J Physiol 581:1019–1031.

Smith MR, Goldin AL (1997) Interaction between the sodium channel inactivation linker and domain III S4–S5. Biophys J 73:1885–1895.

Tang L, Kallen RG, Horn R (1996) Role of an S4–S5 linker in sodium channel inactivation probed by mutagenesis and a peptide blocker. J Gen Physiol 108:89–104.

Tang L, Chehab N, Wieland SJ, Kallen RG (1998) Glutamine substitution at alanine1649 in the S4–S5 cytoplasmic loop of domain 4 removes the voltage sensitivity of fast inactivation in the human heart sodium channel. J Gen Physiol 111:639–652.

Toledo-Aral JJ, Moss BL, He ZJ, Koszowski AG, Whisenand T, Levinson SR, Wolf JJ, Silos-Santiago I, Halegoua S, Mandel G (1997) Identification of PN1, a predominant voltage-dependent sodium channel expressed principally in peripheral neurons. Proc Natl Acad Sci U S A 94:1527–1532.

Waxman SG (2006) Neurobiology: a channel sets the gain on pain. Nature 444:831–832.

Yang Y, Wang Y, Li S, Xu Z, Li H, Ma L, Fan J, Bu D, Liu B, Fan Z, Wu G, Jin J, Ding B, Zhu X, Shen Y (2004) Mutations in SCN9A, encoding a sodium channel alpha subunit, in patients with primary erythermalgia. J Med Genet 41:171–174.